Modeling of HgCdTe Photodetectors in the LWIR region

Pradyumna Muralidharan and Dragica Vasileska
School of Electrical, Computer and Energy Engineering
Arizona State University
Tempe, U.S.A

Priyalal S. Wijewarnasuriya
Sensors and Electron Devices Directorate
U.S Army Research Laboratory
Adelphi, U.S.A

***Abstract*—We have developed a computer program that simulates the electrical characteristics of a p^+ - n HgCdTe photodetector. Using solutions to the Poisson and Continuity equations we investigate low temperature behavior to determine optimum working conditions to enhance detectivity. Our model considers complete Fermi – Dirac statistics, major recombination mechanisms, band to band tunneling, trap assisted tunneling and impact ionization. Device performance was analyzed as a function of doping and temperature. Simulations show detectivity > 10^{11} Jones at 77 K for $Hg_{0.78}Cd_{0.22}Te$.**

Keywords-Infrared detectors; II – VI Semiconductor materials, Tunneling.

I. Introduction

Semiconductor infrared detectors have been a focus for research for over four decades. The realization of high performance infrared detectors over the past few years has enabled applications such as; optical gas sensing, free space communication, infrared counter measures, biomedical and thermal imaging etc. Infrared detectors have found important applications in both military and civilian domains in recent times [1]. To access the wavelength in the infrared region many narrow bandgap materials have been researched. Particularly for this purpose II – VI materials provide great flexibility as they have the capability to function as a wide bandgap as well as narrow a bandgap material. Over the past decade $Hg_{1-x}Cd_xTe$ has firmly established itself as a unique material whose variable cadmium mole fraction can provide bandgap tunability. It is one of the few materials which can detect radiations in the long wavelength (8 – 15 µm), mid wavelength (3 – 8 µm) and the short wavelength (1.4 - 3 µm) infrared region.

Despite the potential applications offered by HgCdTe, there are several design and fabrication obstacles that must be overcome to make an efficient detector. Fabrication of the material with the required purity in itself presents a unique challenge. Growth techniques such as liquid phase epitaxy (LPE) and molecular beam epitaxy (MBE) have been extensively researched to produce high purity HgCdTe. The most crucial challenge that hinders this technology is the operating temperature of the device. To obtain high efficiency, cryogenic cooling is required. LWIR (x = 0.22) detectors must be operated at liquid nitrogen temperatures to obtain background limited performance (BLIP). At lower temperatures the thermally generated noise is highly subdued and the noise generated by the background flux is greater. Significant amount of research has been directed towards reducing the dark current of the device and trying to increase the device operating temperature. Operation at very low temperatures is not the most practical solution as this would greatly increase the overall cost. We have accurately described the Auger generation which is the primary cause of noise and leakage in HgCdTe infrared detectors.

II. Numerical Model

A one dimensional drift – diffusion simulator for homojunctions was developed to simulate the characteristics of a HgCdTe photodetector. We employ complete Fermi – Dirac statistics to compute the electron and hole densities within the device. We conducted simulations on a p^+ - n device as shown in the figure 1 with back illumination.

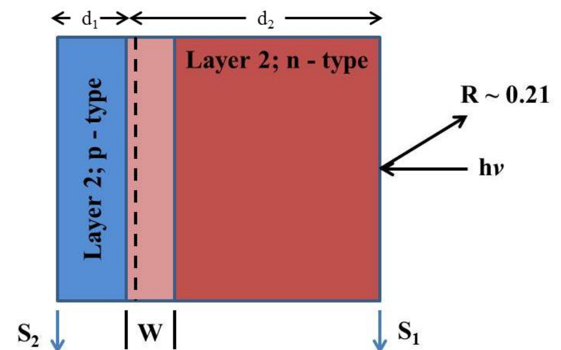

Fig 1. HgCdTe, p^+ - n infrared detector.

A drift – diffusion simulator utilizes the solution to a set of transport equations to describe device behavior. The solutions to a set of continuity equations for electrons and holes, the Poisson equation and all relevant recombination mechanisms are used. The equilibrium poissons equation is given by equation 1. As we are simulating a homojunction we can ignore the spatial variation of the dielectric permittivity.

$$\nabla^2.\varphi = -\frac{e}{\varepsilon}\left(n - p + N_D^+ - N_A^-\right) \qquad (1)$$

Where, N_D^+ and N_A^- are the ionized donor and acceptor concentrations and φ is the electrostatic potential. As we are dealing with a one dimensional problem, we utilize LU decomposition to solve the 1D Poisson's equation on a uniform mesh. To compute current we solve the steady state current continuity equation as given by equation 2 and equation 3.

$$J_n = -q\mu_n n\left(-\frac{d\varphi}{dx}\right) + qD_n\frac{dn}{dx} \quad (2)$$

$$J_p = -q\mu_p p\left(-\frac{d\varphi}{dx}\right) - qD_p\frac{dp}{dx} \quad (3)$$

where, $J_{n,p}$ is the current density, $\mu_{n,p}$ is the carrier mobility and $D_{n,p}$ is the diffusion coefficient. The diffusion coefficient for degenerate materials cannot simply be determined by the Einstein's relation and is therefore determined by Kroemer's expansion [2].

III. Theoretical Model

A. Material Parameters

In $Hg_{1-x}Cd_xTe$ the cadmium mole fraction primarily defines how the material will behave. The formulae to calculate all the basic material parameters such as bandgap, carrier mobility, intrinsic carrier concentration, effective masses and dielectric constants are well known and can be consistently found in literature [3]. All parameters used for our simulations can be found in ref 2. It is noteworthy to mention that all material parameters are highly sensitive to the cadmium mole fraction and temperature.

B. Absorption Coefficient

This is an important parameter in terms of simulation, as it helps to accurately describe the total amount of generation throughout the device. Under conditions of illumination this term can be critical in determining all other parameters. The absorption region is characterized by two particular regions, namely the Kane region, which describes the absorption for all energies above the conduction band edge and the Urbach region, which describes the absorption for all energies below the conduction band edge [4]. The Kane region represents all the band to band transitions. There is a certain amount of absorption even below the conduction band edge due to electron – phonon, electron – impurity and interactions with intermediate trap states. Both regions have been well researched and are well documented in literature [5]. The Urbach absorption obeys an exponential law whereas the Kane region obeys a square root law. Equation 4 and 5 describe this model.

$$\alpha = \beta\sqrt{E - E_g} \quad (4a)$$

$$\beta = -1 + 0.083T + (21 - 0.13T)x \quad (4b)$$

where, x is the cadmium mole fraction and T is the temperature.

$$\alpha = \alpha_0 \exp\left(\frac{\sigma_0 (E - E_0)}{T + T_0}\right) \quad (5a)$$

$$\sigma_0 = 3.267 \times 10^4 (1 + x) \quad (5b)$$

$$E_0 = (1.838x) - 0.3424 \quad (5c)$$

$$T_0 = 81.9 \quad (5d)$$

where x is the cadmium mole fraction. Fig 2 shows the absorption coefficient for $x = 0.20, 0.3, 0.4$.

Fig 2. Absorption Coefficient vs. Energy for $x = 0.2, 0.3, 0.4$.

C. Quantum Efficiency

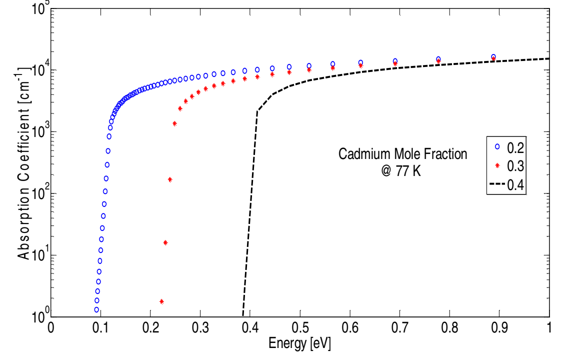

Quantum efficiency (QE) is a term that describes the amount of electron hole pairs that are collected for every incident photon. The major factors that can affect the quantum efficiency and the collection of carriers are; the photosensitive area (the bulk), the depletion region width and the minority carrier depletion region. Equation 6 describes the quantum efficiency based on the minority carrier diffusion length and equation 7 describes the depletion region quantum efficiency [6].

For $d > L_p$

$$\eta = (1 - R)\left[1 - \exp(\alpha(\lambda)d)\right] \quad (6a)$$

For $d < L_p$

$$\eta = (1 - R)\left[\frac{\alpha(\lambda)L_p}{1 + \alpha(\lambda)L_p}\right] \quad (6b)$$

where, α is the absorption coefficient, 'R' is the reflection coefficient ≈ 0.22 and L_p is the diffusion length.

$$\eta_{DR} = (1 - R)\left\{\exp(-\alpha x_n) - \exp\left[-\alpha(x_n + W)\right]\right\} \quad (7)$$

where, W is the depletion width. Ref 5 describes the nature of equation 7 more explicitly. Fig 3 describes the overall quantum efficiency and we see how the QE deteriorates as the absorber region exceeds the minority carrier diffusion length ($L_p \approx 15$ µm). This is due to the fact that carriers lying one diffusion length away from the depletion region do not get collected and therefore cannot be detected. Thus for maximizing the quantum efficiency, the diffusion length is always greater or equal to the bulk thickness. Fig 4 describes the depletion region quantum efficiency.

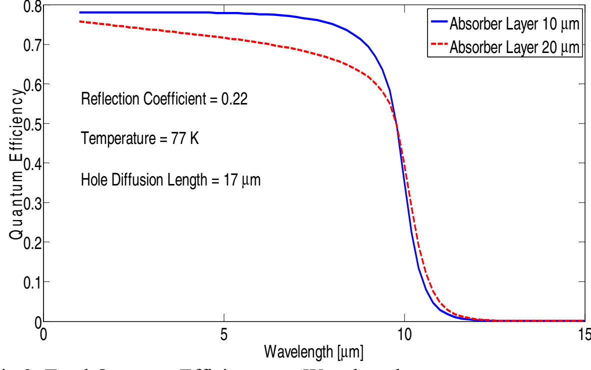

Fig 3. Total Quantum Efficiency vs. Wavelength.

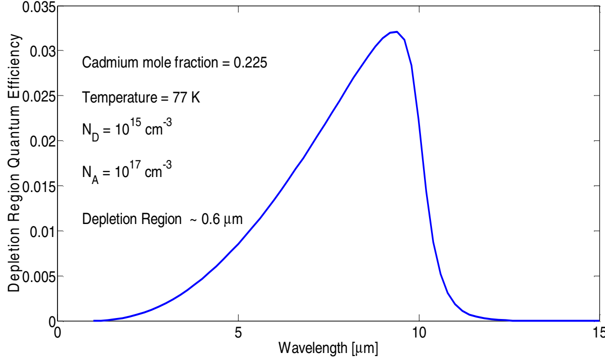

Fig 4: Depletion region QE vs. Wavelength.

D. Recombination Mechanisms

We have considered the SRH, Radiative and Auger mechanisms in our model. SRH recombination can be given by equation 8.

$$R_{SRH} = \frac{pn - n_i^2}{\tau_p(n + n_i \exp\frac{E_t - E_i}{kT}) + \tau_n(p + n_i \exp\frac{-E_t + E_i}{kT})} \quad (8)$$

where, 'E_t' is the trap level, 'E_i' is the intrinsic Fermi energy and '$\tau_{n,p}$' are the carrier lifetimes. The standard definition of Auger and Radiative recombination is used. The optical coefficient in Radiative recombination and the Auger coefficients 'C_n' and 'C_p' are given in ref 7.

The Auger generation is a critical parameter which affects all other parameters in a HgCdTe detector. The intrinsic Auger lifetime is given by equation 9.

$$\tau_A^i = \frac{3.8\times10^{-18}\varepsilon^2(1+\eta)^{1/2}(1+\eta)}{\left(\frac{m_e^*}{m_0}\right)|F_1F_2|^2\left(\frac{kT}{E_g}\right)^{3/2}} \exp\left[\frac{(1+2\eta)}{(1+\eta)}\frac{E_g}{kT}\right] \quad (9)$$

where, 'FF' is the overlap integral and 'η' is m_n^*/m_p^*.

E. Band to Band Tunneling

As HgCdTe is a narrow bandgap material being operated in reverse bias, the probability for tunneling increases with increasing reverse bias. We use a convenient expression using the W.K.B approximation [8] which can easily be implemented for the purpose of drift – diffusion simulations which is given by equation 10.

$$G_T(x) = \frac{\sqrt{2}q^2\sqrt{m^*}F_x^2}{4\pi^2\hbar\sqrt{E_g}} \exp\left[\frac{-\pi\sqrt{m^*}E_g^{3/2}}{2\sqrt{2}q\hbar F_x}\right], \quad (10)$$

where, 'G_T' is the tunneling expressed as a generation rate and 'F_x' is the local electric field. We can see the effects of tunneling in figure 5.

F. Trap Assisted Tunneling

Trap assisted tunneling could become a significant mechanism if the trap states are ideally positioned in the mid gap, and coupled with high electric fields this could lead to deviations from the expected I – V characteristics. The trap assisted tunneling can be expressed as a slight modification of equation 8 by adding a field effect factor '$\Gamma_{n,p}$' [9].

$$R_{SRH} = \frac{pn - n_i^2}{\frac{\tau_p}{1+\Gamma_p}[n + n_i \exp(\frac{E_T - E_i}{kT})] + \frac{\tau_n}{1+\Gamma_n}[p + n_i \exp(\frac{E_i - E_T}{kT})]} \quad (11)$$

G. Detectivity and Responsivity

The detectivity is one of the critical parameters of merit which describes the how powerful the detector is. This term is defined by equation 10. Detectivity is measured in jones.

$$D^* = \frac{n\lambda q}{hc}\left[\frac{4kT}{R_0A} + 2q^2\eta P_{OPT}\right]^{-2} \quad (12)$$

The current responsivity of the device is given by:

$$R = \frac{\lambda}{(hc)F_F}J_{ph} \quad (13)$$

where, 'F_F' is the photon flux at the front surface and 'J_{ph}' is the current under illumination.

H. Impact Ionization

Due to heavy doping and the narrow bandgap nature of the device, very high electric fields are present in the device. The high energy carriers can cause impact ionization. In the local field theory the equation that governs electron and hole impact ionization is given by equation 14 [10].

$$G_{ION} = \frac{1}{q}\alpha_e J_e + \frac{1}{q}\alpha_h J_h \quad (14)$$

Where, '$\alpha_{e,h}$' are functions of electric field and '$J_{e,h}$' are electron and hole currents. '$\alpha_{e,h}$' can be given by equation 15.

$$\alpha_h(F) = a_h \exp\left(-\frac{b_h}{F^{m_h}}\right) \quad (15a)$$

$$\alpha_e(F) = a_e \exp\left(-\frac{b_e}{F^{m_e}}\right) \quad (15b)$$

In equation 15a and 15b, the coefficients '$a_{e,h}$' and '$b_{e,h}$' are given in ref 11.

IV. Results

The dark current is given in figure 5. The simulation shows the I – V characteristics at 70 K, 78 K and 100 K.

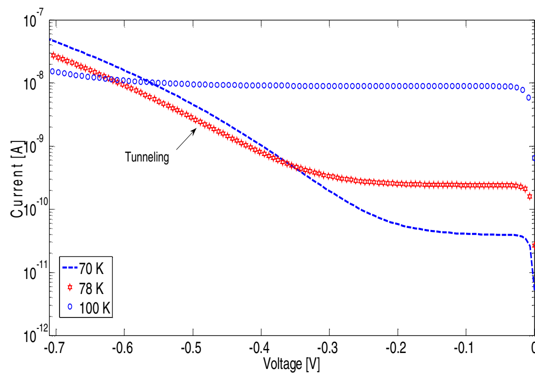

Fig 5. Reverse biased I – V characteristics of a HgCdTe photodetector.

The bandgap of $Hg_{1-x}Cd_xTe$ increases with temperature, and we can notice that effect of tunneling is far more prominent at lower temperatures. At lower voltages (near zero), Auger generation is the primary cause of all the leakage current, this however changes with the application of higher voltages where tunneling becomes dominant. We have also added the effect of ionized dopants, which would ideally lead to carrier freezeout at lower temperatures, but as the donor levels tend to lie deep inside the conduction/valence band, complete ionization is observed even at 77 K.

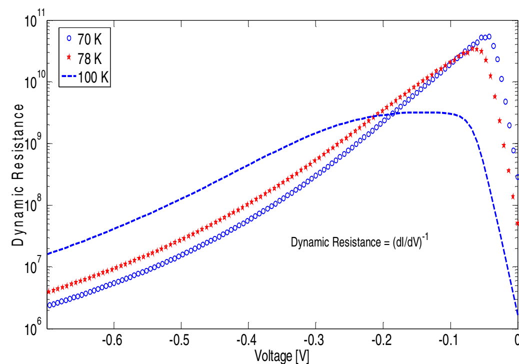

Fig 6. Dyanmic Resistance vs. Voltage at 70K, 78K and 100K

We notice from the above graph the high resistance at low temperatures due to very low dark currents, but at 100 K we notice that the peak dynamic resistance drops to around 10^9 Ω from 10^{11} Ω at 70 K. The noise levels in the device continue to increase as with the increase of temperature and voltage. The increase in temperature leads to higher Auger generation; there are also noticeable contributions of shot noise and Johnson noise. Figure 7 shows the Detectivity (jones) at 77K and 100K. We notice that the Detectivity is an order of magnitude higher at 78K. As the temperature increases the components contributing to noise like Auger generation deteriorate the detectors performance by increasing the leakage current and the detector ceases to provide background limited performance. Thus it is imperative to operate HgCdTe photodetectors at low temperatures.

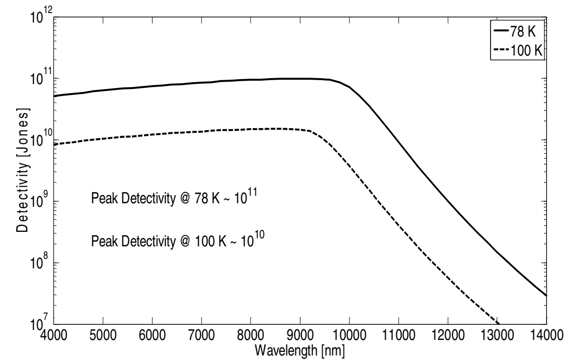

Fig 7. Detectivity vs. Wavelength at 78K and 100K

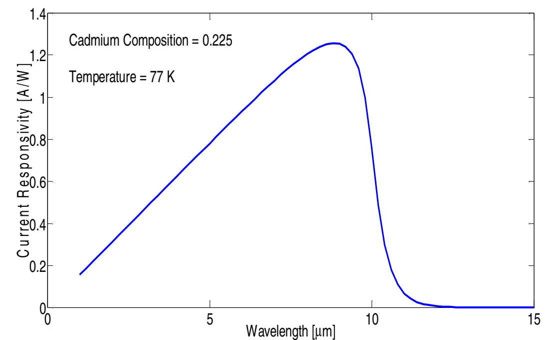

Fig 8. Current Responsivity vs. Wavelength

References

[1] A.Krier, "Mid-infrared Semiconductor Optoelectronics", Springer Series in Optical Sciences, pp. 3-8, 2006.

[2] H. Kroemer, "The Einstein relation for degenerate carrier concentrations", IEEE Trans. Elec. Devices, vol. 25, no. 7, pp. 850, July 1978.

[3] V. Srivastav, R.Pal, V. Venkataraman, "Performance study of high operating temperature HgCdTe mid wave infrared detector through numerical modelling", J. Appl. Phys. 108, 073112, 2010.

[4] B. Li, J.H. Chu, Y. Chang, Y.S. Gui, and D.Y. Tang, "Optical absorption above the energy band gap in $Hg_{1-x}Cd_xTe$", Infrared Phys. 32,195, 1991.

[5] E. Finkman and S.E. Schacham, "The exponential optical absorption band tail of $Hg_{1-x}Cd_xTe$ ", J. Appl. Phys., 56, 2896,1984.

[6] A. Roglaski, K. Adamiec, J. Rutkowski, "Narrow-gap Semiconductor Photodiodes", SPIE, (2000).

[7] A.M Itsuno, J.D Phillips, S. Velicu, "Predicted performance improvement of Auger suppressed HgCdTe photodiodes and heterojunction detectors", IEEE Trans. Elec. Devices, vol.58, no.2, pp. 501-507, 2011.

[8] K. Jozwikowski, M Kopytko, A. Rogalski, A. Jozwikowska, "Enhanced numerical analysis of current – voltage characteristics of long wavelength infrared n-on-p HgCdTe photodiodes", J. Appl. Phys., vol. 108, no. 7, 2010.

[9] G.A.M Hurkx, D.B.M Klassen, M.P.G Knuvers, F.G O'Hara, "A new recombination model describing heavy doping effects and low temperature behaviour", Proc. Int. Elec. Device Meeting, pp. 307-310, 1989.

[10] R.J Mcintyre, "A new look at impact ionization – Part I: A theory of gain, noise, breakdown probability, and frequency response", IEEE Trans. Elec. Devices, vol. 46, no.8, pp. 1623-1631, 1999.

[11] M.A Kinch, "Fundamentals of infrared detector materials", SPIE, 2007.